ISSN 0965-5441, Petroleum Chemistry, 2020, Vol. 60, No. 7, pp. 773–784. © Pleiades Publishing, Ltd., 2020.
Russian Text © The Author(s), 2020, published in Neftekhimiya, 2020, Vol. 60, No. 4, pp. 488–500.

Detection of Steady State Multiplicity during Dimethyl Ether Conversion Catalyzed by $ZnO/\gamma\text{-}Al_2O_3$ Composite: Effect of Coke and Hydrogen Peroxide

A. L. Maksimov[a], V. F. Tret'yakov[a, *], and R. M. Talyshinskii[a]

[a] *Topchiev Institute of Petrochemical Synthesis, Russian Academy of Sciences, Moscow, 119991 Russia*

**e-mail: tretjakov@ips.ac.ru*

Received October 18, 2019; revised November 29, 2019; accepted March 12, 2020

Abstract—The heterogeneous catalytic conversion of dimethyl ether (DME) to 1,3-butadiene and butylenes in the presence of a $ZnO/\gamma\text{-}Al_2O_3$ catalyst in a wide range of temperatures, feed space velocities, and reactant concentrations has been studied. It has been found that temperature regions of 380–420 and 440–480°C, which are conventionally designated as low-temperature and high-temperature regions, differ in the laws governing the occurrence of the process associated with the specificity of coking of the catalyst surface and a redistribution of the surface concentration of Brønsted and Lewis acid sites. A hypothesis of a change of the catalytic process mechanism upon the transition of the reaction into the high-temperature region has been put forward and confirmed by the occurrence of a hysteresis detected in this temperature range. The effect of hydrogen peroxide on the hysteresis parameters and the steady state stability during DME conversion has been shown.

Keywords: steady state multiplicity, catalysis, DME, 1,3-butadiene, butylenes, carbon deposits, hysteresis, coke, thermal desorption, acidity

DOI: 10.1134/S0965544120070087

INTRODUCTION

An acute problem of catalytic chemistry is the formation of condensation products (coke) on the surface of heterogeneous catalysts on stream; these products block the active sites of the catalysts and cause a loss of activity, selectivity, and instability.

The specificity of the coking processes that occur on a heterogeneous surface of solid catalysts frequently leads to the occurrence of a steady state multiplicity (SSM) in the reaction systems and difficulties in controlling the reaction process parameters in an optimum mode.

The key tasks in eliminating these problems to restore the main performance characteristics of heterogeneous catalysts are the stabilization or restoration of their chemical and phase composition and structural and textural characteristics.

However, it should be stated that the currently available methods to regenerate the surface of spent catalysts do not fully meet all requirements of modern technologies for the catalytic production of chemicals.

Thus, a commonly used method to regenerate spent catalysts by a periodic thermal oxidative treatment, i.e., coke burning-off in an air stream (in the presence or absence of steam), frequently leads to sintering of the catalytically active component. As a consequence, the specific surface area of the catalyst decreases and the pore structure changes; these factors, in turn, require a frequent refreshment of the catalytic charge, which is economically unreasonable [1–3].

In this aspect, a fairly urgent task is the search for fundamentally new methods to extend the time between regenerations of deactivating catalysts that would not lead to undesirable and irreversible changes in their characteristics. These methods include, for example, the catalyst system self-regeneration method based on the introduction of compounds (e.g., hydrogen peroxide) into the reaction medium composition that inhibit the formation of condensation products and coke on a heterogeneous surface and stabilize the steady state during reaction [4].

Currently, owing to the shortage in the production of synthetic rubber monomers, the use of carbon-containing feedstocks alternative to oil, in particular, oxygenates, such as ethanol, methanol, and dimethyl ether (DME), is significantly expanding [5–7].

Earlier [8–10], it has been first shown that one of the important monomers of heavy organic synthesis—1,3-butadiene—can be actually produced from DME in the presence of a modified $ZnO/\gamma\text{-}Al_2O_3$ catalyst via the intermediate conversion of DME to ethanol,

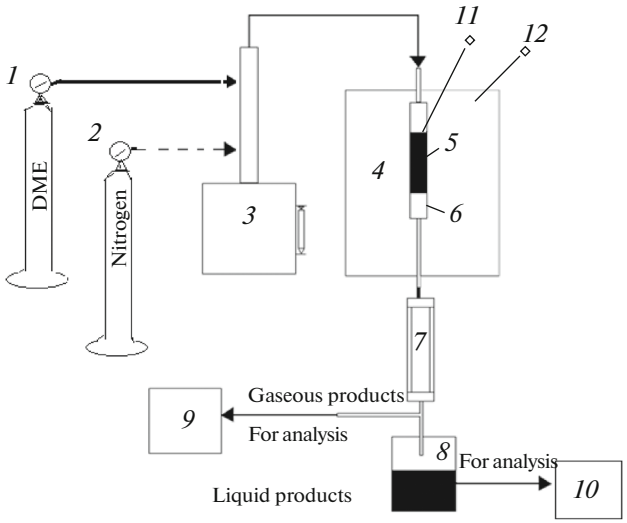

Fig. 1. Diagram of a flow system for testing the catalyst activity: (*1, 2*) cylinders containing DME and nitrogen, (*3*) dosing pump for feeding liquid reactants, (*4*) oven, (*5*) catalyst bed, (*6*) reactor, (*7*) refrigerator, (*8*) condenser, (*9, 10*) Kristallyuks-4000M chromatographs to analyze gas and liquid phases, (*11*) load thermocouple in the catalyst bed, and (*12*) control thermocouple of the oven.

which is further converted to butadiene in accordance with the known mechanism discovered by Lebedev [11]. A kinetic model to satisfactorily describe the revealed relationships in the considered temperature range was proposed in [10].

However, it should be noted that, unlike the above conversion of ethyl alcohol to butadiene, DME conversions are accompanied by a relatively high degree of coking of the catalyst surface, which leads to a rapid loss of initial activity, the formation of a variable-composition catalyzate, and a significant decrease in the time between regenerations.

This study is focused on the relationship between the characteristics of the proposed $ZnO/\gamma\text{-}Al_2O_3$ catalyst for DME conversion to divinyl and the coking of the catalyst surface, the effect of hydrogen peroxide additives to the feed stream on the regeneration of the active sites of the catalyst to remove carbon deposits, and the establishment of a respective steady state during reaction.

EXPERIMENTAL

The effect of DME conversion mode parameters was studied in a quartz reactor with a catalyst load of 10 mL on the system shown in Fig. 1 in a temperature range of 380–480°C at a DME gas hourly space velocity (GHSV) of 100–190 h^{-1} with dilution of the feedstock with nitrogen in a molar ratio of 2.0 : 1 to 11.5 : 1. The catalyst-bed temperature gradient at a load of 5–10 mL was ±5°C. The qualitative and quantitative composition of the synthesized catalysts was analyzed chromatographically as described in [8].

Dimethyl ether conversion rate was calculated by the formula

$$W_{\text{DME}}^{\Sigma} = \frac{\alpha}{100} Wo, \quad (1)$$

where α is the DME conversion (%) and *Wo* is the DME feed rate (mol/(L h)).

The tests were repeated to determine reproducibility; the data were averaged. The standard deviations from the average rate values for the system components did not exceed Δ = ±7%. Reaction rate was normalized to 1 L of catalyst per hour; it is shown in terms of mol/(L h).

The catalyst was synthesized by the diffusion impregnation of γ-alumina with zinc and aluminum nitrate solutions at 200–500°C and subsequent drying and calcining of the precursors under conditions described in [9, 10].

Aluminum nitrate taken in an amount to provide 10 wt % in the final formulation was introduced into the system to form a strong bond between the zinc and aluminum oxides.

Prior to using, γ-alumina was calcined at 600°C for 6 h and then placed in a desiccator, where it was cooled to room temperature. The support was impregnated with active component solutions at 80°C for 3 h. The amount of the active component solution was calculated by the incipient wetness impregnation method with the addition of a required amount of distilled water.

The impregnated wet support was emulsified at 20°C for 12 h; after that, the sample was heated to 120°C and dried under stirring for 2 h to prevent the precursor particles from coalescence. Next, after the addition of an aqueous solution of tartaric acid at a pH of 2.5 by the incipient wetness impregnation method, the catalyst was further dried in a desiccator for 10 h.

The synthesized sample was placed in a muffle furnace, where it was calcined at 200 and 300°C for 2 h at each temperature; after that, it was cooled to room temperature in a desiccator. Ammonia water was added by the incipient wetness impregnation method. After stripping nitrogen oxides in a muffle furnace at 350°C, the catalyst precursor in a required amount was placed into the reactor, where the sample was calcined and simultaneously activated at 400 and 550°C in alternating streams of nitrogen, air, and hydrogen (2 L/h per 5 mL of sample) for 3 h. The catalyst formulation was calculated in terms of oxide content: 22.5 wt % ZnO and 77.5 wt % $\gamma\text{-}Al_2O_3$.

Special tests on variation in the linear velocity of the feed stream [8] in a range of 5–10 cm/s and the fractional composition of the catalyst granules in a range of (0.2–0.3)–(0.8–1.0) mm showed that external and internal diffusion does not have any effect

during DME conversion in the studied range of variation in the reaction process parameters.

The textural characteristics of the catalyst samples were studied on a unified Sorbi-MS system by the low-temperature nitrogen adsorption method and calculated by the Brunauer–Emmett–Teller (BET) method. Total sorption pore volume V_Σ (total volume of micro- and mesopores) was determined from the amount of nitrogen adsorbed at a relative pressure close to unity on the assumption that all the pores were filled with nitrogen in the condensed state due to capillary condensation. In this case, the adsorbed nitrogen volume (V_Σ) was converted into the liquid nitrogen volume (V_{liq}) using the following equation:

$$V_{liq} = \frac{P_A V_\Sigma V_M}{RT}, \quad (2)$$

where P_A and T are the ambient pressure and temperature, respectively; V_M is the molar volume of liquid nitrogen ($V_M = 34.7$ cm^3/g); and R is the gas constant.

The acidic properties of the catalyst surface were determined by the temperature programmed desorption (TPD) of ammonia and infrared (IR) spectral analysis of adsorbed ammonia and carbon monoxide molecules as probe molecules.

The total surface acidity of the samples was determined under the assumption of single-site ammonia adsorption from the number of chemisorbed molecules, the desorption of which was almost completed upon an increase in the temperature in the column with the catalyst to 600°C.

The total number of acid sites N_Σ (unit/m^2) was calculated from the values of the area under the desorption curves by the formula

$$N_\Sigma = \frac{6.02 \times 10^{23} \sum T_{max_i}}{22400 \times S_{sp} G}, \quad (3)$$

where 6.02×10^{23} is the Avogadro number; S_{sp} is the specific surface area of catalyst samples, m^2/g; G is the weighed portion of the catalyst, g; and $\sum T_{max_i}$ is the total peak area on the thermal desorption curve, mm^2, which is proportional to the desorbed volume of gaseous ammonia V, mL. The number of moles of desorbed ammonia was calculated as $V/22400$, where 22400 is the volume of one mole of NH_3.

The differential thermal analysis (DTA) of the support and catalyst samples (fresh and coked) and their precursors was conducted on a Q-1500 D derivatograph (F. Paulik, J. Paulik, L. Erdey; MOM, Hungary); the linear heating rate was 7.5–10.0°C/min.

Thermogravimetric analysis (TGA) was conducted in an air atmosphere or a nitrogen atmosphere. The weighed portions of the samples were 120–250 mg (weighing error of ±0.4 mg). Temperature was measured using a platinum/platinum–rhodium thermocouple (PP-1) with an accuracy of ±2°C in a temperature range of 22–900°C.

X-ray diffraction patterns were recorded on a DRON-3 automated X-ray diffractometer with a graphite monochromator. Measurements were conducted using CuK_α radiation in the step-by-step scanning mode in increments of $2\theta = 0.1°$. The acquisition time was 3 s per point. The diffraction patterns were processed using the PHAN and PHAN (%) software programs for qualitative and quantitative X-ray diffraction analyses.

Infrared spectra were recorded at an adsorption temperature on a Shimadzu 8300 Fourier transform IR spectrometer at a resolution of 4 cm^{-1} and a spectrum accumulation factor of 50. The freshly prepared samples were precompressed into pellets with a density of 7–17 mg/cm^2, calcined in an IR cell at 450°C in a vacuum (0.013–0.001 MPa) for 1 h, and then cooled to 110°C with liquid nitrogen. Acid sites were identified using ammonia and carbon monoxide as probe molecules.

RESULTS AND DISCUSSION

Table 1 shows characteristics of the specific surface area and porosity of the ZnO/γ-Al_2O_3 catalyst samples synthesized for testing in DME conversion. It is evident that their final textural characteristics are determined by the parameters of the selected support. However, the introduction of zinc oxide into the matrix of the support leads to a certain decrease in the specific surface area and total pore volume. An increase in the zinc oxide content in the catalyst samples leads to a redistribution of pore volume with respect to size, namely, a decrease in the number of micro- and mesopores and an increase in the number of macropores.

According to the diffraction patterns shown in Fig. 2, the observed change in the textural characteristics of the ZnO/γ-Al_2O_3 catalysts with an increase in the zinc oxide content is apparently attributed to the formation of a zinc aluminate phase and the increase in the relative content of this phase, which affects the degree of development of the active surface of the samples.

The initial data used to calculate the total and partial DME conversion rates were a sample of results of the chromatographic analysis of the component composition of the reaction products at a reaction temperature varied in a range of 380–480°C, a DME GHSV of 100–190 h^{-1}, and a nitrogen : feedstock molar ratio of (1–10) : 1 (Table 2).

According to the above data and the results of studying the kinetic laws of the reaction described in [10], the most probable sequence of DME conversion to the target reaction product—1,3-butadiene—that occurs in the high temperature region of 420–480°C is the following:

Table 1. Dependence of textural characteristics of the γ-Al_2O_3 support and the ZnO/γ-Al_2O_3 catalysts on heat treatment conditions

ZnO/Al_2O_3 catalyst sample	Heat treatment conditions T, °C/time, min		S_{sp}, m^2/g	V_{pore}, cm^3/g	Pore volume distribution by pore size, nm		
	thermolysis	calcining			5–10	10–10^2	10^2–10^3
γ-Al_2O_3*	–	–	188	0.58	0.23	0.27	0.08
ZnO (5.0%)	320/120	430/240	178	0.55	0.21	0.24	0.10
ZnO (10%)	320/150	450/240	168	0.52	0.18	0.22	0.12
ZnO (15%)	320/180	450/300	165	0.50	0.16	0.21	0.13
ZnO (20%)	320/150	450/300	153	0.47	0.13	0.15	0.19

* The support before the deposition of the active mass.

$$CH_3OCH_3 \longrightarrow C_2H_5OH \begin{matrix} \nearrow CH_3CHO \\ + \\ \searrow CH_2{=}CH_2 \end{matrix} \longrightarrow CH_2{=}CH{-}CH{=}CH_2. \quad (4)$$

In the low-temperature reaction region, the sequence of formation of divinyl is apparently implemented in accordance with the Lebedev mechanism [11]:

$$2CH_3OCH_3 \rightarrow 2C_2H_5OH \rightarrow 2CH_3CHO \rightarrow CH_3CHOH{-}CH_3CHO \rightarrow CH_3CH{=}CHCHO \rightarrow CH_2{=}CH{-}CH{=}CH_2. \quad (5)$$

Comparison of the activity of the freshly prepared catalyst samples and the samples after use on-stream for 7 h and more (Table 3) revealed a change in the DME conversion rate and routes, which was not observed in the early period of manifestation of activity. It was found that the most significant differences in these behaviors are observed with a change of the temperature regions of the process, which are conventionally designated as low-temperature (380–420°C) and high-temperature regions (440–480°C). In addition, upon transition from the boundary point of the low-temperature region (420°C) to the high-temperature region (480°C), the relative decrease in the total DME conversion rate and the reaction product yield is more pronounced.

It is noteworthy that at the maximum reaction temperature in the studied range (480°C), the introduction of hydrogen peroxide in an amount of 1.5 wt % with respect to DME into the feed stream contributes to the restoration of the catalyst activity; therefore, the rates of the total and partial DME conversions almost approach the values listed in Table 2; in this case, a

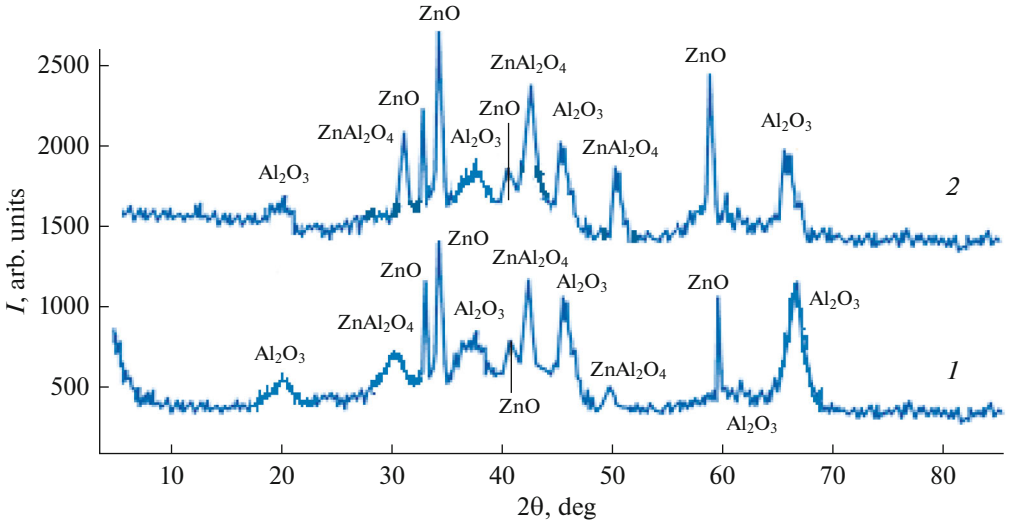

Fig. 2. X-ray diffraction patterns of ZnO/Al_2O_3catalyst samples. Zinc content in the samples: (*1*) 10 and (*2*) 20 wt % in terms of oxides.

Table 2. Dependence of the total DME conversion rate $\left(W_{\mathrm{DME}}^{\Sigma}\right)$ and the product yield ($\alpha \times S_i$) on DME GHSV at a reaction temperature varied in a range of 420–480°C and a DME : N_2 molar ratio of 1 : 10 in the presence of a $ZnO/\gamma\text{-}Al_2O_3$ catalyst

GHSV, h^{-1}	Total conversion rate $W_{\mathrm{DME}}^{\Sigma}$, mol/(L h)	DME conversion α, %	Reaction product yield in the contact gas ($\alpha \times S_i$), %								
			divinyl	*n*-butylene	ethanol	acetaldehyde	ethylene	propylene	diethyl ether	formaldehyde	$CO + CH_4$
Contact zone temperature, 380°C											
100	1.96	44.0	19.3	0	4.5	0	10.0	0	0	0.34	4.3
150	2.28	34.0	20.0	3.0	5.9	0.44	33.5	2.9	4.6	0.29	6.1
190	2.54	30.0	19.2	3.3	8.3	0.23	38.8	2.3	4.0	0.27	7.0
Contact zone temperature, 400°C											
100	2.14	48.0	20.0	0	27.1	0	19.6	0	0	0.52	19.4
150	2.55	38.0	20.2	3.8	4.3	0.5	28.3	3.4	3.9	0.40	19.3
190	2.97	35.0	18.3	12.0	2.86	0.29	27.8	2.86	2.2	0.34	21.0
Contact zone temperature, 420°C											
100	2.39	53.5	19.4	3.7	15.9	0	18.9	0	0.2	0.37	17.2
150	2.88	43.0	19.5	9.3	6.42	0.42	24.0	3.2	3.5	0.19	29.6
190	3.22	38.0	18.9	11.8	5.18	0.23	21.7	3.15	1.3	0.16	31.3
Contact zone temperature, 440°C											
100	2.55	57.2	15.3	0	12.3	0	18.0	0.1	0.3	0.2	23.5
150	3.25	48.5	15.6	6.7	0.3	0.35	22.5	3.2	3.4	0.1	30.4
190	3.60	42.4	14.8	7.0	0.2	0.15	19.3	2.9	1.0	0	33.6
Contact zone temperature, 460°C											
100	2.70	60.5	10.2	0	0	0	17.6	0	0	0.1	28.3
150	3.44	51.3	10.5	6.2	0.1	0.21	21.0	3.0	3.2	0	36.7
190	3.82	45.0	9.6	5.9	0	0.1	16.6	2.8	0.5	0	40.2
Contact zone temperature, 480°C											
100	2.79	62.4	7.8	1.8	5.2	2.6	7.3	1.6	0.9	0	31.2
150	3.66	54.6	8.0	5.6	5.8	2.9	11.0	2.5	2.3	0	39.6
190	4.07	48.0	7.4	5.1	3.3	2.7	8.0	2.0	0.1	0	42.4

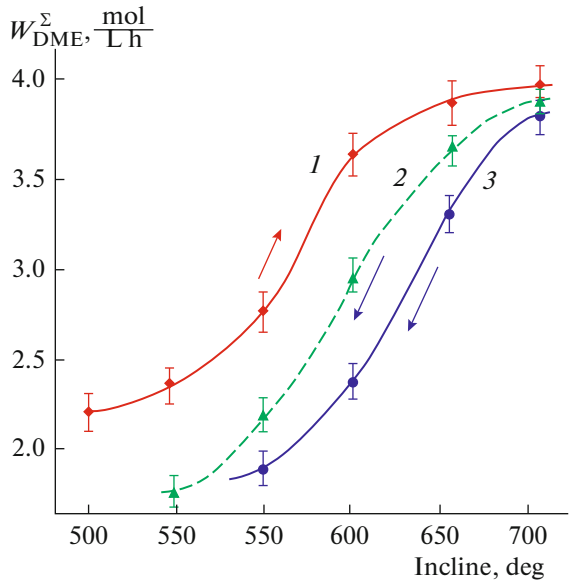

Fig. 3. Temperature dependence of the total DME conversion rate: (*1*) the original $ZnO/\gamma\text{-}Al_2O_3$ catalyst sample, (*2*) the catalyst sample after the completion of the reaction run, and (*3*) DME conversion after the completion of the reaction run with the introduction of 1.5 wt % of hydrogen peroxide. Reaction conditions: GHSV = 190 h^{-1}; time of DME conversion to the next measurement of the DME conversion rate, 1 h.

small amount of carbon dioxide is identified in the gaseous portion of the catalyzate. In addition, upon transition from the boundary point of the low-temperature region (420°C) to the high-temperature region (480°C), the relative decrease in the total DME conversion rate and the reaction product yield is more pronounced.

It is noteworthy that at the maximum reaction temperature in the studied range (480°C), the introduction of hydrogen peroxide in an amount of 1.5 wt % with respect to DME into the feed stream contributes to the restoration of the catalyst activity; therefore, the rates of the total and partial DME conversions almost approach the values listed in Table 2; in this case, a small amount of carbon dioxide is identified in the gaseous portion of the catalyzate.

In the high-temperature reaction mode, the transition of DME conversions into the diffusion region or the occurrence of heterogeneous–homogeneous post-catalytic volumetric conversions were eliminated after special tests; therefore, the most probable cause of the change in the catalytic activity is the specificity of coking of the catalyst surface.

To confirm the above assumption on the cause of the change in the mechanism of DME conversions upon transition to the high-temperature region, comparative tests of the activity of the catalysts were conducted after a certain time of contacting with the reaction medium.

The processing of the experimental data revealed the presence of a hysteresis in the W_{DME}/T_{PEAK} coordinates (Fig. 3); the hysteresis is apparently due to a change of the mechanism of surface DME conversion, which is determined by a change in the pattern of the active surface of the catalyst.

During the tests, the total DME conversion rate in the presence of a freshly prepared catalyst at 380°C was initially determined (first point in curve *1*). After 1 h, the rate was measured again (second point in curve *1*). Upon achieving a reaction temperature of 440°C, at the fourth point in curve *1* (transition of the reaction to the high-temperature region), the temperature dependence of the DME conversion rate abruptly deviates from the nearly exponential behavior and the further increase in the rate decreases. It is obvious that, within the final time of the reaction run (sixth point in curve *1*), coke accumulates in a certain amount providing the blocking of the active surface sites of the catalyst; it is this factor that causes the decrease in the catalyst activity. It is characteristic that, with a stepwise decrease in the reaction temperature (curve *2*) and reversion to the points identified in temperature curve *1*, a significant discrepancy in the DME conversion rate is observed; that is, an S-shaped temperature hysteresis takes place.

It was found that the introduction of H_2O_2 in an amount of 1.5 wt % into the reaction mixture and the subsequent stepwise decrease in temperature leads to a partial restoration of the catalyst activity (curve *3*). In this case, the difference in the activity of the freshly prepared and coked samples becomes less significant; that is, in this case, hydrogen peroxide exhibits the regenerating function as an oxidizer of carbon deposits.

A direct evidence of the formation of carbon deposits during DME conversion of in the presence of ZnO/Al_2O_3 catalysts was obtained by DTA of the catalyst samples after a 10-h continuous run of the system (Fig. 4).

The results show that, during the heating of the samples, their weight gradually decreases; this decrease is accompanied by several exothermic effects associated with the burnout of the surface carbon deposits. The occurrence of two maxima in the DTA curves in a temperature range of 450–500 and 500–550°C (sample *1*) and 350–400 and 400–450°C (sample *2*) indicates the presence of two types of deposits that differ in the strength of the bond to the surface of the catalyst samples.

According to DTA of the catalyst samples, after a 10-h run of the system with the addition of hydrogen peroxide to the feed stream, the exothermic peaks corresponding to the two types of carbon deposits decreased; this finding confirms that H_2O_2 exhibits a coke formation regenerating function during DME conversion.

Table 3. Dependence of the total DME conversion rate $\left(W_{\text{DME}}^{\Sigma}\right)$ and the product yield ($\alpha \times S_i$) on DME GHSV at a reaction temperature varied in the range of 420–480°C and a DME : N_2 molar ratio of 1 : 10 in the presence of $ZnO/\gamma\text{-}Al_2O_3$ catalysts after a 7-h continuous on-stream of the freshly prepared samples

GHSV, h^{-1}	Total conversion rate W_{DME}^{Σ}, mol/(L h)	DME conversion α, %	Product yield in contact gas ($\alpha \times S_i$), %								
			divinyl	*n*-butylene	ethanol	acetaldehyde	ethylene	propylene	diethyl ether	formaldehyde	$CO + CO_2 + CH_4$
Contact zone temperature, 420°C											
100	2.05	37.0	13.5	2.2	13.7	1.2	14.2	2.0	0.4	0.22	18.3
150	2.23	32.0	14.3	3.5	6.2	0.24	20.5	2.8	2.7	0.15	30.3
190	2.58	27.0	13.2	6.3	4.1	0.15	17.7	3.0	1.2	0.11	28.3
Contact zone temperature, 480°C											
100	2.23	44.0	5.5	0	27.1	0	19.6	0	0	0.52	19.4
150	2.56	33.0	4.9	3.8	4.3	0.5	28.3	3.4	3.9	0.40	19.3
190	2.97	28.0	4.3	12.0	2.86	0.29	27.8	2.86	2.2	0.34	21.0
Contact zone temperature, 480°C*											
100	2.57	58.0	7.4	1.6	5.0	2.3	6.8	1.5	0.7	0.2	38.4
150	3.08	48.0	7.6	5.3	5.4	2.2	9.6	2.4	2.0	0	43.2
190	3.72	45.0	7.2	4.7	2.9	2.5	7.8	1.9	0	0	48.6

* The tests were conducted with the introduction of 1.5 wt % of hydrogen peroxide into the feed stream.

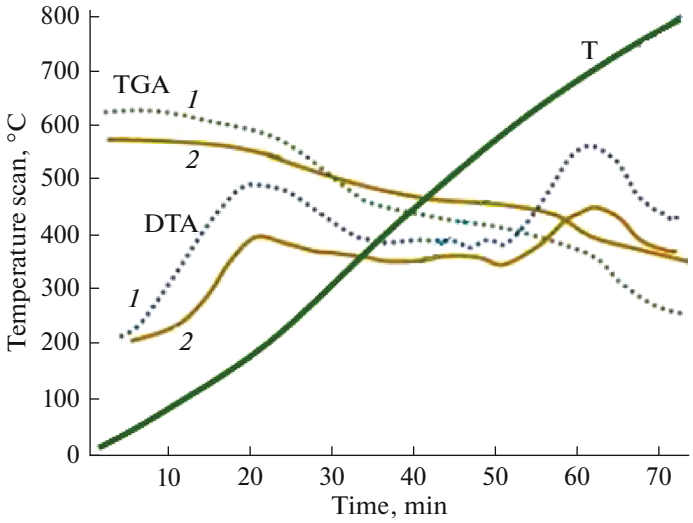

Fig. 4. Thermogravimetric analysis and DTA curves of $ZnO/\gamma\text{-}Al_2O_3$ catalysts after 10-h runs of the system (*1*) in the absence of H_2O_2 additives and (*2*) in the case of introduction of 1.5 wt % hydrogen peroxide into the reaction zone.

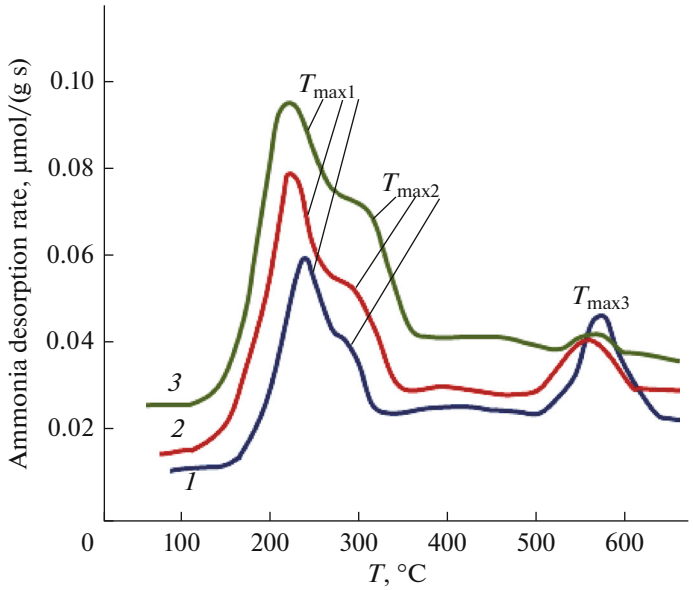

Fig. 5. Ammonia TPD spectra of the surface of (*1*) the $\gamma\text{-}Al_2O_3$ support and ZnO/Al_2O_3 catalyst samples with a ZnO content in the support matrix of (*2*) 10 and (*3*) 20 wt %.

The described results suggest that the formation of carbon deposits on the catalyst surface involves at least two types of active—presumably acid—sites localized in the $\gamma\text{-}Al_2O_3$ support matrix.

The TPD spectra of ammonia adsorbed on the surface of the $\gamma\text{-}Al_2O_3$ support of the active mass of potential $ZnO/\gamma\text{-}Al_2O_3$ catalysts (Fig. 5, Table 4) exhibit three desorption maxima that change their position on the temperature coordinate depending on the experimental conditions, °C: T_{max_1} (145–235), T_{max_2} (240–290), and T_{max_3} (500–550).

The observed maxima correspond to the desorption of ammonia from surface acid sites, which are conventionally classified as weak, medium-strength, and strongly acidic sites.

The above data suggest that the introduction of zinc oxide into the alumina support matrix leads to a quantitative redistribution of acid sites.

Thus, an increase in the content of the active mass (ZnO) leads to the blocking of acid sites of all three types and a decrease in their number; these effects are also evident as a shift of the maxima of the ammonia desorption peaks (T_{max_i}) to the low temperature region

Table 4. Comparison of the surface acidity characteristics of the γ-Al_2O_3 support and ZnO/γ-Al_2O_3 catalysts calculated from ammonia TPD spectra: initial temperature of NH_3 adsorption, 50–65°C; programmed heating rate, β = 10–20 °C/min; and NH_3 dosage, 0.1–0.5 mmol

Support and ZnO/Al_2O_3 catalyst samples*	Temperature T_{max_i}			Acidity corresponding to T_{max_i}			$\sum N_i \times 10^{19}$ unit/m^2
	T_{max_1}	T_{max_2}	T_{max_3}	N_1	N_2	N_3	
γ-Al_2O_3	145–235	240–290	500–550	1.20×10^{19}	6.72×10^{18}	9.58×10^{18}	2.83
ZnO, 10%	140–225	233–285	490–545	1.26×10^{19}	7.08×10^{18}	3.52×10^{18}	2.32
ZnO, 20%	133–210	230–280	485–540	1.25×10^{19}	6.25×10^{18}	2.75×10^{18}	2.15
ZnO, 10%**	135–220	225–275	470–520	1.12×10^{19}	5.75×10^{18}	1.25×10^{18}	1.82
ZnO, 10%***	138–220	235–280	492–547	1.28×10^{19}	6.65×10^{18}	3.25×10^{18}	2.27

* The support before the deposition of the active mass.
** The catalyst after a 10-h run of the system.
*** The catalyst after a 10-h run of the system with the introduction of H_2O_2 into the feed stream.

(see Fig. 5). In this case, the number of strong acid sites undergoes the most significant decrease.

A similar acid site redistribution was observed during the thermal desorption of ammonia from the coked surface of ZnO/Al_2O_3 catalysts that were in contact with the reaction medium after a 10-h run of the system.

To determine the Brønsted acidity of the original γ-Al_2O_3 support and ZnO/γ-Al_2O_3 catalyst samples, the absorption spectra of OH groups that occur in the region of 3400–3800 cm^{-1} (bridging and terminal OH groups) were analyzed (Fig. 6).

It is evident from the spectrum parameters of the support that before the deposition of the active mass of zinc oxide (*1*), the OH groups peaking at the highest frequencies (ν_{OH} = 3775 cm^{-1}), which are apparently bound to tetrahedral aluminum ions, and the OH groups (ν_{OH} = 3725 cm^{-1}) bound to octahedral aluminum ions can be classified as terminal groups.

The other OH groups giving bands in the low-frequency region of the spectrum (ν_{OH} = 3670–3570 cm^{-1}) are bridging groups localized between differently coordinated aluminum ions.

An increase in the amount of the deposited ZnO active mass (spectra *2, 3*) leads to a shift of the absorp-

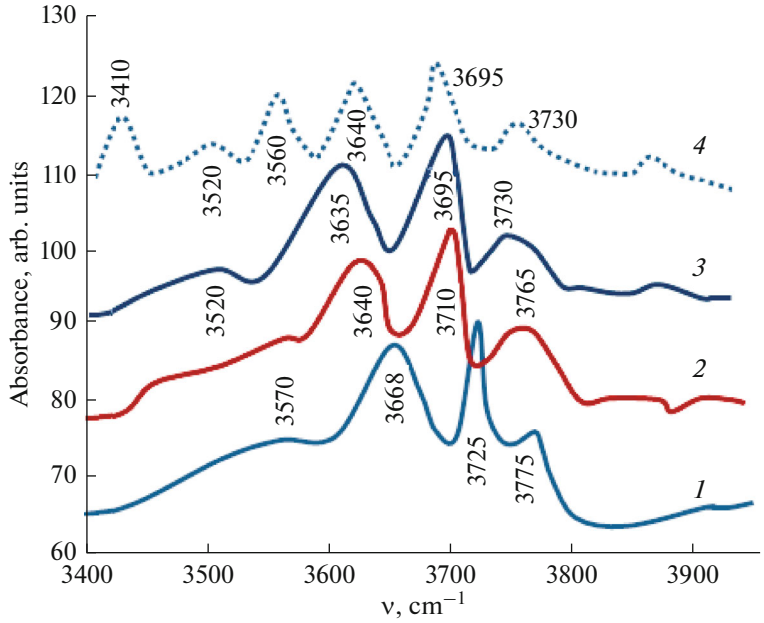

Fig. 6. Fragments of IR spectra of (*1*) the γ-Al_2O_3 support and ZnO/Al_2O_3 catalyst samples in a wave number region of 3900–3400 cm^{-1} (absorption by OH groups). Zinc oxide content in the γ-Al_2O_3 matrix: (*2*) 10 and (*3*) 20 wt %; (*4*) after feeding ammonia into the cell.

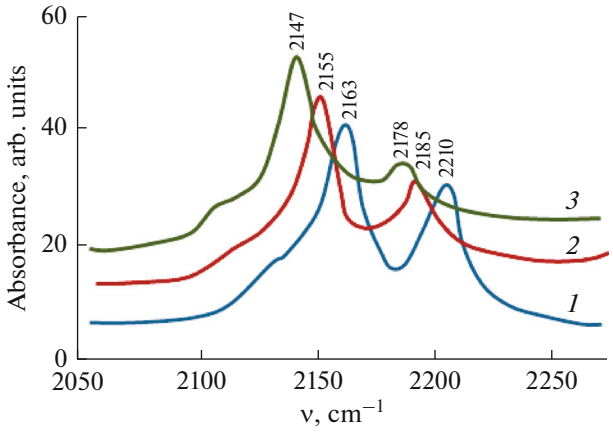

Fig. 7. Infrared spectra of carbon monoxide adsorbed on the surface of (*1*) the γ-Al_2O_3 support and ZnO/Al_2O_3 catalysts with a ZnO content in the sample of (*2*) 10 and (*3*) 20 wt %.

tion bands of OH groups to the low-frequency region and a simultaneous increase in their relative intensity, which is attributed to the partial neutralization of stronger Brønsted acid sites on the surface of the samples.

After feeding a dosed amount of ammonia into the measuring cell, the IR spectra of the sample containing 20 wt % ZnO in the support matrix show a decrease in the intensity of the absorption bands of free hydroxyl groups at 3695 and 3730 cm^{-1} and the simultaneous appearance of bands at 3560 and 3410 cm^{-1}, which is characteristic of the formation of a hydrogen bond between NH_3 molecules and proton-donating Brønsted acid sites on the catalyst surface.

The absorption spectra of carbon monoxide adsorbed on the surface of the γ-Al_2O_3 support and ZnO/Al_2O_3 catalysts precalcined at 500–550°C indicate the presence of two types of Lewis acid sites that differ in strength; the sites are characterized by CO absorption bands in the regions of 2150–2170 and 2180–2210 cm^{-1}, respectively (Fig. 7).

It is evident that, with an increase in the zinc cation concentration, the absorption bands corresponding to both strong and weak Lewis acid sites are shifted to the low-frequency region. In this case, a decrease in the intensity of the absorption bands characteristic of the strongly acidic sites of the original γ-Al_2O_3, a redistribution of the surface concentration of acid sites, and the appearance of new absorption bands corresponding to weaker acceptor sites (2155 and 2147 cm^{-1}) are observed.

Thus, the data on DME conversion in the presence of freshly prepared ZnO/γ-Al_2O_3 catalysts and the catalysts coked during reaction, the IR data of probe molecules adsorbed on the catalyst surface (NH_3 and CO), and the DTA data for the samples suggest that there are two temperature regions of the reaction, namely, 380–420 and 440–480°C. In each of these regions, a certain sequence of formation of the target product—1,3-butadiene—is dominant in accordance with the above schemes (3) and (4); that is, depending on reaction conditions, the presence of an SSM is observed; in the case under consideration, two steady states take place.

The presence of two steady states during the DME conversion reaction suggests that the reaction mechanism in the above temperature regions is also multichannel; it is not improbable that the slow stages change with temperature variation. In this case, it is assumed that the active Brønsted and Lewis acid sites are mostly involved in the reaction in the low-temperature and high-temperature regions, respectively.

A similar mechanism most probably takes place despite the following fact revealed by X-ray diffraction analysis: in the entire studied temperature range, the phase composition of the samples is constant regardless of the degree of coking of the catalyst surface after reaction.

CLOSING REMARKS

Along with studying the kinetic mechanism for the implementation of processes, it is necessary to thoroughly study their dynamics associated with both macroscopic factors and critical phenomena in catalysis that are caused by SSM, surface coking, self-vibration modes, etc. This study showed that macrokinetic factors do not significantly affect the DME conversion process. The hysteresis detected in the temperature range examined indicates the presence of an SSM caused by the presence of two types of sites (Brønsted and Lewis).

The results make it possible to accelerate the prediction of the catalyst design and effectively implement the process on an industrial scale. Note that most reports in the field of heterogeneous catalysis do not provide data on nonlinear effects and SSM; the lack of these data impedes the development of science and production in the chemical industry.

The evolution of heterogeneous catalytic conversions in porous media is associated with multiphase processes [12–15], which are evident in the dynamics of reactions apparently attributed to the interplays of the catalyst and the initiator, which forms the catalyst system under the conditions of catalyst surface coking. A deeper understanding of the catalytic process mechanism makes it possible to predict the catalyst genesis determined by the chemical composition and synthesis algorithm of the catalyst.

The relationship between the catalyst genesis and the kinetic parameters of reactions was studied in [17–21], where it was shown that by varying catalyst synthesis parameters, it is possible to affect the activation

energy and the factors of interaction of reactants with active surface sites.

Note that aluminum was used as a binder in the $ZnO + Al_2O_3$ binary system in [5–7]. There are common approaches in the synthesis that are in accordance with the results for the catalyst samples synthesized in this study. For example, impregnation is practiced by the diffusion of a mixed solution of active components containing zinc and aluminum, which are deposited on alumina, and air-drying at room temperature for 12 h. This procedure is aimed at strengthening the bond between zinc and aluminum oxides. The desired final result of strengthening the bond between the metals would be the formation of the $ZnAl_2O_4$ spinel. Typically, spinels are formed at fairly high temperatures above 1000°C. However, Elam et al. [6] reported the presence of a spinel despite that the highest calcining point did not exceed 500°C. At the same time, regardless of the presence of a spinel in the system, according to [5–7, 22], zinc dissolves in a zinc–aluminum mixture and strengthens the bond between the metal oxides.

Thus, the current fundamental ideas on heterogeneous catalysis can be expanded and developed not only owing to solving the practical problem of catalyst synthesis, but also owing to a deeper understanding of the mechanism including the kinetics and dynamics of the process [21].

Note that the chemistry of catalytic DME conversion in terms of the effect on the SSM mechanism was not studied in [8–10]; therefore, the revealed relationships required a more detailed study.

The results of this study suggest that the dynamics of processes catalyzed by composites based on aluminum and zinc oxides used in various reactions involving oxygenates should be studied in detail [7, 22–24]. Typical objects for studying these effects are multiroute reactions that occur in accordance with nonlinear mechanisms complicated by a significant yield of byproducts and coking of the catalyst surface [25–33]; this fact should be taken into account to implement industrial petrochemical processes.

CONCLUSIONS

(i) It has been found that DME conversion occurs in two temperature regions exhibiting different tendencies in affecting the mode parameters; this finding indicates the existence of different mechanisms of the reaction and the presence of an SSM.

(ii) The presence of an SSM is evidenced by the occurrence of a hysteresis loop between the detected temperature regions of the reaction in the temperature range of 380–420°C.

(iii) The revealed steady states are characterized by stability, which is enhanced upon the initiation of the process by hydrogen peroxide.

(iv) It has been found that, during DME conversion, an SSM takes place; it is attributed to the presence of coke on the surface of a catalyst containing a $ZnO/\gamma\text{-}Al_2O_3$ binary composite and controlled by the ratio of Lewis and Brønsted sites depending on the process temperature.

FUNDING

This work was performed under a state task of the Topchiev Institute of Petrochemical Synthesis of the Russian Academy of Sciences.

CONFLICT OF INTEREST

A.L. Maksimov is the editor-in-chief of the *Neftekhimiya* (Petroleum Chemistry) journal. The other authors declare that there is no conflict of interest to be disclosed this paper.

REFERENCES

1. A. A. Lamberov, I. N. Mukhambetov, and R. F. Zalyaliev, Catal. Ind. **6**, 128 (2014).
2. R. Hughes, *Deactivation of Catalysts* (Academic, London, 1984).
3. N. V. Ostrovskii, *Catalyst Deactivation Kinetics: Mathematical Models and Their Application* (Nauka, Moscow, 2001) [in Russian].
4. V. F. Tret'yakov and R. M. Talyshinskii, *Kinetics and Dynamics of Heterogeneous Catalyzed Petrochemical Processes* (MITKhT, Moscow, 2012) [in Russian].
5. D. Liu, Y. Men, J. Wang, et al., Am. J. Anal. Chem. **7** (7), 568 (2016).
6. J. W. Elam, A. D. Routkevitch, and S. M. George, J. Electrochem. Soc. **150**, 339 (2003).
7. M. A. Kipnis, I. A. Belostotskii, E. A. Volnina, and G. I. Lin, Catal. Ind. **11**, 53 (2019).
8. S. N. Khadzhiev, A. L. Maksimov, V. F. Tret'yakov, et al., Pet. Chem. **58**, 405 (2018).
9. A. L. Maksimov, V. F. Tret'yakov, R. M. Talyshinskii, et al., Neftegazokhimiya **59** (2), 44 (2019).
10. A. L. Maksimov, V. F. Tret'yakov, Yu. N. Litvishkov, et al., Khim. Probl., No. 1, 135 (2019).
11. S. V. Lebedev, *Life and Works* (ONTI Khim. Teoret., Leningrad, 1938) [in Russian].
12. V. I. Bykov, *Modeling of Critical Phenomena in Chemical Kinetics* (KomKniga, Moscow, 2006) [in Russian].
13. G. S. Yablonskii, V. I. Bykov, and A. N. Gorban', *Kinetic Models of Catalytic Reactions* (Nauka, Novosibirsk, 1983) [in Russian].
14. B. S. Gudkov, A. N. Subbotin, and V. I. Yakerson, *Temperature Hysteresis in Heterogeneous Catalysis* (Khimiya, Moscow, 2001) [in Russian].
15. A. I. Boyarinov, *Multiplicity of Steady States in the Mixer–Reactor–Separation Unit System* (Khimiya, Moscow, 1982) [in Russian].
16. S. N. Khadzhiev, V. F. Tret'yakov, A. M. Ilolov, and R. M. Talyshinskii, Nanotekhnol., Nauka Proizvod. **1** (10), 33 (2015).

17. A. M. Gyul'maliev, V. F. Tret'yakov, R. M. Talyshinskii, et al., Pet. Chem. **59**, 979 (2019).
18. Yu. N. Litvishkov, P. A. Muradova, M. R. Efendiev, et al., Khim. Probl., No. 2, 290 (2009).
19. V. F. Tret'yakov, R. M. Talyshinskii, K. V. Tret'yakov, et al., Neftepererab. Neftekhim., No. 12, 44 (2011).
20. S. L. Kiperman, *Foundations of Chemical Kinetics in Heterogeneous Catalysis* (Khimiya, Moscow, 1979) [in Russian].
21. A. L. Maksimov, V. F. Tret'yakov, and R. M. Talyshinskii, Neftegazokhimiya, No. 4, 34 (2018).
22. Kh. M. Kadiev, M. Kh. Kadieva, L. A. Zekel', et al., Colloid J. **81**, 90 (2019).
23. M. Cai, V. Subramanian, V. V. Sushkevich, et al., Appl. Catal., A **502**, 370 (2015).
24. V. L. Sushkevich, I. I. Ivanova, and E. Taarning, Green Chem. **17**, 2552 (2015).
25. O. N. Temkin, *Lectures Notes in the Theory of Mechanisms of Complex Reactions and Catalysis* (Moscow, 2003) [in Russian].
26. T.G. Alkhazov, and L.Ya. Margolis, *High-Level Catalytic Oxidation of Organic Substances* (Khimiya, Moscow, 1985) [in Russian].
27. L. G. Bruk and O. N. Temkin, Kinet. Catal. **57**, 277 (2016).
28. P. Debye, *Selected Works* (Nauka, Leningrad, 1987) [in Russian].
29. A. V. Myshlyavtsev and M. D. Myshlyavtseva, Kinet. Catal. **48**, 541 (2007).
30. V. Kh. Fedotov, N. I. Kol'tsov, and B. V. Alekseev, Dokl. Akad. Nauk SSSR **302**, 126 (1988).
31. L. I. Kheifets and A. V. Neimark, *Multiphase Processes in Porous Media* (Khimiya, Moscow, 1982) [in Russian].
32. I. Ya. Mittova, A. A. Samsonov, and B. V. Sladkopevtsev, *Basic Concepts and Mechanisms of Catalytic and Coupled Reactions: Nonequilibrium Processes in Catalysis (Classical Systems)* (Izd. Voronezhskogo Gosudarstvennogo Univ., Voronezh, 2012) [in Russian].
33. F. A. Yandieva, M. V. Tsodikov, A. V. Chistyakov, et al., Kinet. Catal. **51**, 548 (2010).

Translated by M. Timoshinina